

## LCLS-II STATUS, ISSUES AND PLANS\*

M. C. Ross<sup>†</sup>, SLAC National Accelerator Laboratory, Stanford, CA 94305, USA

### Abstract

The Linac Coherent Light Source II (LCLS-II) project requires the assembly, test, and installation of 37 cryomodules (CM) in order to deliver a 4 GeV CW electron beam to the FEL undulators for production of both hard and soft X-ray pulses at a repetition rate of up to 1 MHz. SRF cavity performance in the 30+ tested CM exceeds gradient and cryogenic dynamic heat-load requirements (set at 16 MV/m and 10 W resp). In this talk we present microphonics, shipping, magnetic-flux exclusion, and field emission performance. The US funding agency, DOE, has recently approved an additional 20 CM for the extension of LCLS-II to 8 GeV. This paper will also include initial cavity and heat-load performance results for the extension project, LCLS-II-HE.

### INTRODUCTION

The LCLS-II Free Electron Laser (FEL) project [1] takes advantage of the excellent performance of the LCLS FEL [2] and the successful development of superconducting RF technology, done in part in preparation for a future linear collider [3,4]. Following the completion of the International Linear Collider (ILC) Technical Design Report [5] in 2013, a partnership of US accelerator labs initiated the US Department of Energy (DOE) Critical Decision (CD) process and quickly obtained permission to baseline and start procurements for the roughly 1.04 billion USD project. Completion (CD-4) is planned for 30 June 2022.

Table 1: Performance of Large (>100 m) CW SRF Linacs. The bottom row of the table shows the improvement in cryogenic heat load per GeV of acceleration over ~27 years.

Parameter	CEBAF 1994	LEP2 1999	LCLS-II 2021
N_cav	338	288	280
$E_{acc}$ (MV/m)	7.5	7.2	18.5
Meters of SRF	169	490	296
$E_{tot}$ (GeV)	1.2	3.6	4.6
$\langle Q0 \rangle$	4.0e9	3.2e9	2.7e10
f (MHz)	1497	352	1300
Temp (K)	2.08	4.5	2.0
Heat Load(kW)	5	53	3.7
Heat Load /GeV	4.2	14.7*	0.8

\* @4.5K. Divide by 3.5 to convert to equivalent load at 2 K, (4.2 for LEP2)

\* Work supported by US DOE Contract DE-AC02-766SF00515

<sup>†</sup> email address mcrec@slac.stanford.edu

LCLS-II is the first application of low cryogenic-loss nitrogen doping SRF technology [6]. Nitrogen doping reduces the high purity niobium ‘BCS’ resistance ( $R_{BCS}$ ) by a factor of three to four enabling large CW accelerator facilities to operate with 15-20 MV/m acceleration gradients ( $E_{acc}$ ). The doping is applied to the now-standard 1300 MHz nine-cell niobium sheet elliptical cavity. Table 1 compares large ~100 m linac performance over the last roughly 27 years and shows the factor of five impact that nitrogen doping has had on heat load.

Table 2 shows the LCLS-II Machine parameters. Figure 1 shows the layout of the LCLS-II SRF linac (from the end of the injector), housed in the first kilometer of the SLAC infrastructure formerly used for the normal-conducting linac. Each cavity is powered by its own 4.8 kW solid-state amplifier (SSA) with nominal loaded Q ( $Q_{ext}$ ) of  $4e7$ , considered a practical match of low beam current and anticipated microphonics.  $Q_{ext}$  can be manually adjusted within a +/- factor 3 range.

Cryogens for the facility are provided by two independent 4kW (at 2.0K) helium refrigerators, based closely on the five-stage full cold compression Jefferson Lab CHL-2 design, commissioned in 2012 [7]. The complex is expected to be loaded to capacity following the completion of LCLS-II-HE; only one of the two is required for LCLS-II. A ~300 m long two-arm cryo distribution system (CDS) feeds cold helium to the cryomodule strings [8]. Two distribution boxes (labeled DB in Fig. 1), each containing a 2-4 K heat exchanger, are located in the surface building directly above the cryomodule connection points.

### European XFEL

The SRF technology deployed for LCLS-II follows very closely that developed and constructed for the European XFEL. Niobium, cavity, coupler, cryomodule, and auxiliary components are mechanically almost identical to that used for the recently completed European XFEL (XFEL) [9]. Changes to the cavity higher-order-mode extractor, fundamental power coupler (FPC), cavity tuner, and magnetic shielding were required to manage the 1) higher dynamic heat load, 2) higher  $Q_{ext}$ , 3) higher average beam current, and 4) higher sensitivity to magnetic field. ( $B_{amb}$ ). The CM hardware was fabricated by many of the same companies and was tested by institutes that have close collaborative relationships with XFEL institutes. The most-important collaborators from outside the DOE system are DESY, CEA/Saclay, INFN (Milano), and KEK.

### DOE Office of Science Lab Partnership

Fermilab and Thomas Jefferson Lab (JLab) each constructed and tested roughly half of the 37 cryomodules (35 each 1.3 GHz CM and two each 3.9 GHz linearizer CM).

Content from this work may be used under the terms of the CC BY 3.0 licence (© 2019). Any distribution of this work must maintain attribution to the author(s), title of the work, publisher, and DOI.

In addition, the JLab cryogenics group designed and managed the production of the 2.0 K cryoplant and Fermilab provided the cryogenic distribution system. SLAC was responsible for integration of the linac, cryoplant, and cryogenic distribution system.

### LCLS-II-HE

In 2018, the same partnership initiated the CD process for LCLS-II-HE to make X-rays up to 12.8 keV [10]. The new project received CD-1 (approval of the conceptual design and cost-range) in September 2018. Twenty CM with an improved doping scheme and higher  $E_{acc}$  of 20.8 MV/m will be built from 2021 to 2023 using the same partnership scheme as for LCLS-II. A prototype will be built and tested at Fermilab in 2020. Figure 1 shows the LCLS-II-HE layout.

Table 2: LCLS-II Machine Parameters

Parameter	Value	Units
Energy	4	GeV
Beam I	100	$\mu$ Amp
Duty Factor	CW	
RF	1300	MHz
Cavity	8	per CM
Cryomodules	35	each
Linearizer CM	2	each
Cryoplant cap.	8	kW@2.0K
SSA	4.8	kW

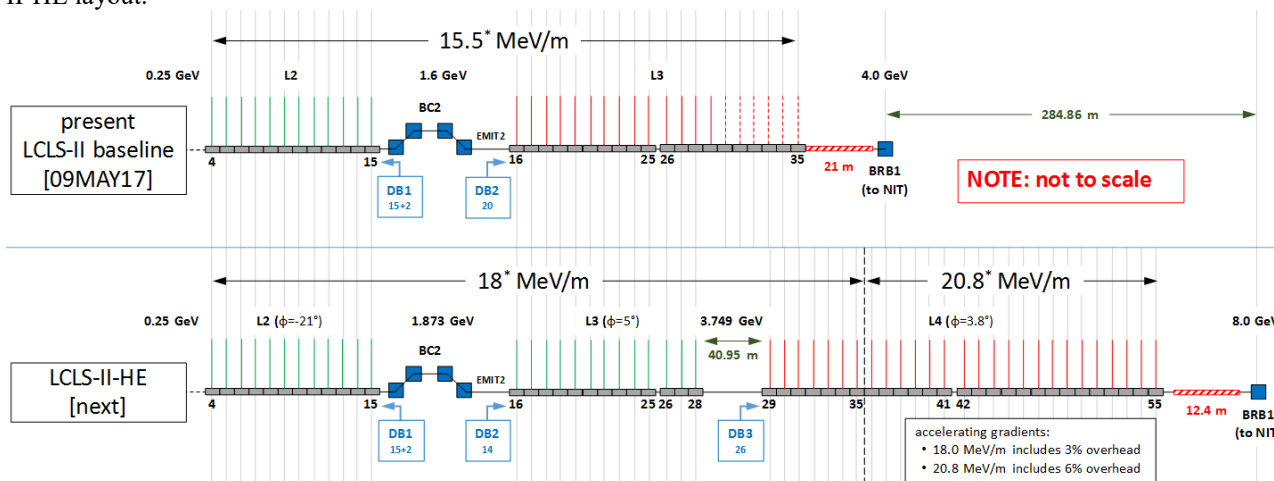


Figure 1: LCLS-II (top) and LCLS-II-HE (bottom) SRF linac layout schematic. (The injector and BC1 are omitted).

## SUPERCONDUCTING CAVITIES

Cavity performance for the CW linac has two primary criteria acceptance thresholds for  $E_{acc}$  and  $Q0$  (inverse heat load). In a pulse-mode linac the latter is less important as the overall cryogenic capacity requirement has a much larger relative contribution from the static heat load. Table 3 lists the cavity vertical test (VT) acceptance criteria. The cavity vendors were not responsible for VT performance but were responsible for meeting hold-point requirements (mechanical, surface processing, microwave tuning, integration) and quality assurance reporting.

### Nitrogen Doping

Nitrogen doping, first reported in 2012 by Grassellino et al [6], changes the electron mean free path and the energy band-gap in the superconductor resulting in greatly reduced  $R_{BCS}$ .  $R_{BCS}$  continues to improve with increasing  $E_{acc}$ . Doping is done in two steps at the end of the hydrogen-outgas vacuum heat cycle. First, 25 milli Torr  $N_2$  is established in the high-temperature oven for a few minutes, then, while maintaining temperature, the pressure is quickly reduced for a few minute anneal cycle. The anneal cycle ends when oven cool down begins. Non-superconducting niobium nitride compounds form on the surface

and (ideally) stop forming during the anneal cycle. The atomic nitrogen continues to diffuse deeper into the bulk niobium resulting a nitrogen concentration about 100x background and 30 microns thick. The nitrides do not penetrate and must be completely removed with 5-micron electro-polishing chemistry.

Before starting cavity production, a detailed, well-defined doping/annealing process (including allowable margins) was established through the Q0 R&D Program [11]. The R&D Program benefited from the availability of cavities fabricated for the ILC high gradient study [12]. Eighteen nine-cell cavities were pre-tested to establish a baseline, doped, and re-tested in an industrial-style scheme with a 2 minute dope / 6 minute anneal recipe. Vertical test results were excellent, with  $\langle E_{acc} \rangle = 21.6$  MV/m and  $\langle Q0 \rangle = 3.5e10$ , well above target averages of 16 MV/m and  $2.7e10$  respectively. Sixteen of the 18 were used to build two prototype CM (pCM). Long-term (several year) tests, including to-air vents, show the doping is durable.

### Cavity Industrialization

Cavities were fully fabricated, processed and tuned by two companies, Research Instruments (Germany) and Ettore Zanon (Italy). Following the XFEL scheme [13], cavities are delivered fully dressed in their titanium helium

vessels, under vacuum, and ready for vertical test [14]. Each vendor prepared two cavities, provided by LCLS-II, in a doping-qualification cycle [15]. These were tested at Fermilab and Jefferson Lab with excellent results, indicating nitrogen doping process was ready to begin transfer to industry.

Table 3: Cavity Acceptance Criteria in Vertical Test. ( $Q0$  criterium in VT is reduced by  $0.2e10$  to account for the two blank flanges on the beamline ports.)

Parameters	Numbers	Unit
$E_{acc}$	>19	MV/m
$Q0$	>2.5e10	(at 16 MV/m)
R	<10	n $\Omega$
HOM power	<1.0	W
Field emission	>17.5	MV/m
Onset*		
Field Emission at onset	<1	nA

\*Field Emission limits changed 30% into production to require *No Detectable Field Emission* at maximum gradient

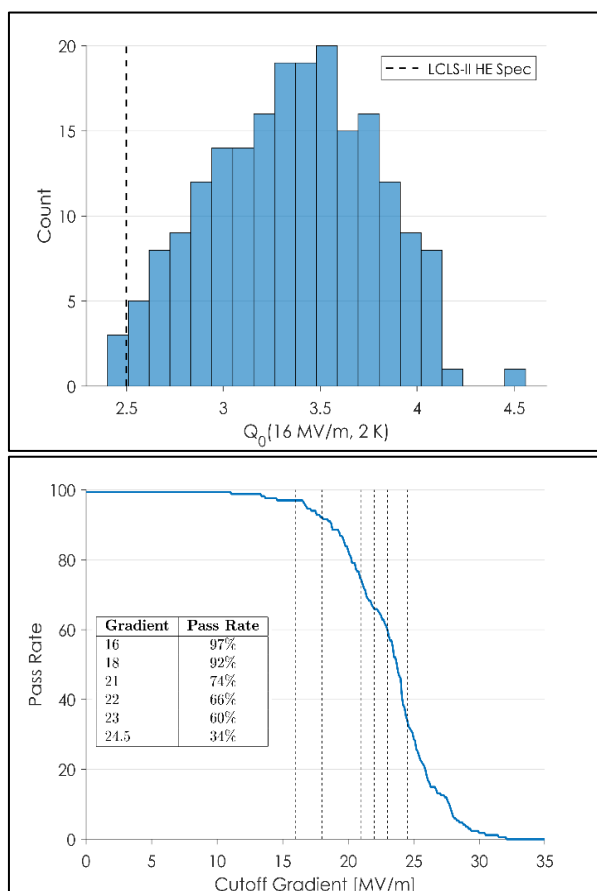


Figure 2: Cavity VT performance.

Initial production at one of the two vendors was plagued with poor performing cavities requiring a remediation program [16].

Figure 2 shows vertical cavity test results for both  $Q0$  and  $E_{acc}$  for cavities with adequate heat treatment and acceptable vendor processing.

## Facilities - Progress

### status report of funded machines

## Magnetic Flux Expulsion

Nitrogen doping causes both a reduced  $E_{acc}$  quench limit compared to the un-doped cavities (>40 MV/m to 27 MV/m) and increased heat dissipation per unit of trapped magnetic flux (roughly 3x, from 0.6 to 1.5 n $\Omega$ /mGauss) [17]. In practice, since typical  $B_{amb}$  in the CM is ~3-5 mGauss, the latter is much more important as it has a direct impact on the cryogenic load of the linac. Two steps are taken to reduce the additional heat: 1) minimizing of  $B_{amb}$  around the cavity and 2) maximizing Meissner-effect magnetic flux expulsion by the superconductor at cool down transition to below  $T_c$  (9.2 K) so that the fraction of  $B_{amb}$  trapped in the cavity is as low as possible. Good flux expulsion efficiency requires a smooth, sweeping cool down through  $T_c$  and, evidently, appropriate bulk niobium metallurgical properties [18,19], so that such a cool down through  $T_c$  traps expels  $B_{amb}$ . Cool down characteristics of cavities in VT and CM are quite different due to cavity orientation and CM cryogenic piping [20]. If slow or non-uniform cavity cool down happens in a CM, for example following a quench, a ‘fast cool down’ (FCD) reset, typically from 40 K with 32 g/s 4K He flow, is required to release trapped flux. Numerical studies have shown this is practical in the fully assembled SLAC linac [21].

Niobium sheet was purchased from two vendors [22] using the specification developed for the JLab 12-GeV upgrade and XFEL projects. Cavities were made of sheets from one vendor or the other, but not of mixed content from both vendors. The first batch of cavities made from sheets from either of the two vendors showed very poor flux expulsion efficiency, even with optimum fast cool down through  $T_c$ . This was identified to be a bulk phenomenon and could be fully corrected by increasing the degas-cycle temperature, (one of the two vendor’s sheets requiring higher temperature to develop full efficiency). Dressed, tuned, cavities cannot be heat treated to such high temperatures and several cryomodules were built with low expulsion efficiency cavities (see Table 4). From that point forward sample sheets from each Nb parent ingot were used to assemble single – cell cavities to prove flux expulsion for that specific material. This is rather expensive and time consuming and efforts are underway to augment the existing specification to include metallurgical criteria aimed at achieving efficient flux expulsion.

Three steps were taken to keep  $B_{amb}$  surrounding the cavity in VT and in the CM to below 5 mGauss. 1) Two layers of hermetic magnetic shielding are placed in the CM around the cavity. 2) All close-in components, (such as the Ti/SUS bimetallic transition joint), and associated tools used for installation, are demagnetized and verified (a practice known as magnetic hygiene) [23]. 3) Each CM subject to a degaussing cycle or cycles [24,25]. The CM are all equipped with between 3 and 5 fluxgate magnetometers. In practice this has been successful and no active  $B_{amb}$  cancellation has been needed in CM test. While the SLAC tunnel is oriented east-west, and the magnitude of  $B_{amb}$  is low compared to the test facilities, sections of it have become magnetized over time and it is unknown if an active

cancellation system will be required in order to stay below the 5 mGauss limit.

## CRYOMODULE

The most important design advances needed to adapt for CW operation have already been summarized [26]. The Fermilab team is the ‘designer of record’. JLab provided mechanical mode and transportation analysis.

Equivalent, and in many cases identical, mass-production tooling was deployed at the production facilities, CEA-Saclay (XFEL), Fermilab and Jefferson Lab (both LCLS-II). Having the two facilities in parallel provided a unique opportunity to compare different institutional procedures and infrastructure performance since incoming procured components and tooling are identical. Some of the differences seen in performance can therefore be attributed to different practice.

For example, JLab keeps the cavity string actively pumped and under vacuum throughout CM assembly. Ideally, cavities are never backfilled throughout the life of the CM. Fermilab practice is to assemble the CM with the string back-filled nitrogen, as like XFEL. The strings are not actively pumped during shipment and installation. As would be expected, the additional integrated pumping time results in better base pressure for the JLab strings (~30x).

Table 4: Cryomodule Acceptance Testing

Parameter	Criteria
Total stable gradient: ~10 hour minimum hold	>16 MV/m average; 128 MV total
Usable $E_{acc}$ . Limit by radiation, quench, or admin. limit	Admin limit: 21 MV/m
Total heat load (@ 2K)	$Q = 2.7 \times 10^{10}$ , 88W
$B_{amb}$	<5 mGauss
Radiation/dark current:	≤10 nA equivalent of radiation @ 16 MV/m (all cavities in phase)
Onset of detectable Field Emission and its magnitude at operating gradient	50 mrad/hr limit for $E_{acc}$ (usable)
Endurance test (all cavities powered)	10-16 hours

### Cryomodule Testing

Cryomodule testing is ‘critical-path’ on the project schedule. Testing infrastructure is expensive, prone to unforeseen shutdown, and may have limited capabilities. Typical ‘good’ CM testing durations (i.e. without unforeseen shutdown) are 28 days, including installation, cool down, soak, testing, warm up and removal. Table 4 lists the CM acceptance requirements. Failure to meet a given criteria triggers a review and mitigation process.

For LCLS-II three test facilities, Cryomodule Test Facility (CMTF, JLab), Cryomodule Test Station-1 (CMTS-1, Fermilab), and Low Energy Recirculator Facility (LERF, JLab) were used. The JLab CMTF, (commissioned ~1990 [27]), required reconfiguration in order to provide 32 g/s

helium as needed for FCD. CM tested before the reconfiguration (J-01 to J-07) show poor flux expulsion and are listed in italics in Table 5. To check that slow cool down indeed caused the high heat load, one CM, (J-01) was tested at both CMTF and CMTS-1.

Each of the 3 facilities were initially configured with very different radiation-dose instrumentation. Since  $E_{acc}$  usable, which is sometimes fixed by the maximum allowable radiation dose rate of less than 50 mrad/hour, is an important limitation to performance, these differences required resolution during production. That process is not complete and it is planned to review and resolve it further during LCLS-II-HE CM production.

Table 5: Cryomodule test results for total usable  $E_{acc}$  (units MV) and average Q0 ( $\times 10^{10}$ ). ‘F-#’ were built and tested at Fermilab, ‘J-#’ at JLab. Twenty-nine out of 35 (not incl 5 each spares) have been tested with an average CM  $E_{acc}$  of 18.5 MV/m and an average Q0 of  $2.8 \times 10^{10}$ . \*J-01 results are from testing done at Fermilab CMTS-1.

CM	$E_{acc}$	Q0	CM	$E_{acc}$	Q0
F-01	151	2.9	J-01	142	2.7*
F-02	166	2.1	<i>J-02</i>	138	1.7
F-03	146	3.4	<i>J-03</i>	134	2.2
F-04	164	3.1	<i>J-04</i>	144	1.9
F-05	158	3.0	<i>J-05</i>	150	2.3
F-06	166	1.9	<i>J-07</i>	130	1.9
F-07	167	2.6	J-08	127	2.5
F-08	162	2.3	J-10	156	3.0
F-09	171	3.3	J-12	161	2.8
F-10	168	2.7	J-13	152	2.7
F-11	163	3.6	J-14	151	2.6
F-12	164	3.0	J-15	146	2.3
F-13	162	3.2			
F-14	150	2.9			
F-15	152	3.0			
F-16	152	3.6			
F-17	141	3.1			

### Field Emission

Ionizing radiation from field emission (FE) causes induced radioactivity and radiation damage [28], in addition to limiting  $E_{acc}$  and increasing cryogenic heat loads. Radiation damage modelling [29] was used to estimate the allowable maximum dark current, minimum  $E_{acc}$  (onset) onset gradient, and maximum radiation dose-rate. Figure 3 shows cavity  $E_{acc}$  (usable) distributions reported by the two CM production lines for a) all cavities (232 each), b) cavities without detectable field emission, and c) cavities with field emission (69). In b), it is clear the two test facilities report the same parent distribution. In c) there may be an indication the JLab CM have a greater incidence of field emission, even though the number of FE cavities is less (29 vs 39). The number of cavities where the maximum gradient is set by field emission is much less than the number shown in Fig. 3 (11 JLab / 9 Fermilab). The figure shows  $E_{acc}$  (usable) for cavities with evidence of field emission.

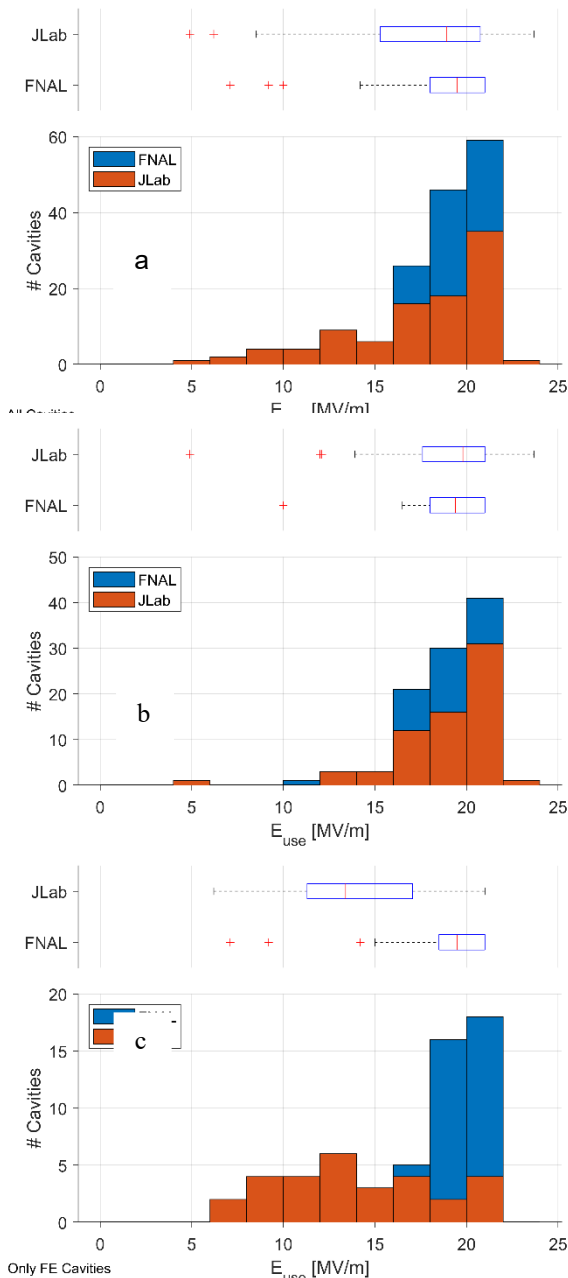


Figure 3:  $E_{acc}$  (usable) in CM test for a) all CM, b) no FE, c) only FE cavities. (The bins are overlaid).

At roughly the 30% point in the production and test cycle, following the scheme of XFEL, cavity string assembly process and infrastructure at both institutes were audited [27,30]. This was successful and subsequent assemblies had substantially reduced FE rates. A total of 6 CM show no detectable FE up to the quench or admin limit.

### Multi-pactor breakdown

The TESLA elliptical cross-section cavity is known to have a multipactor discharge band from 17 to 23 MV/m [31]. A typical discharge event may cause quench and the subsequent return to the superconducting state may result in increased trapped flux giving a higher heat load to 2K. A sequence of such events, for example during processing,

can ratchet up trapped flux leading to an ever-increasing heat load, eventually requiring an FCD reset [32]. This depends on  $B_{amb}$  and the size of the normal-conducting zone. Multipactor processing will be required as a part of commissioning in the assembled linac in order to keep the heat load fixed and limit the rate of FCD resets [33].

### Microphonic Instability

Initial testing of LCLS-II cryomodules showed high amplitude microphonic instability in the low sub-audio band [34] that was ultimately traced to thermo-acoustic oscillations (TAO) in the two cryogenic valves built into each cryomodule (see Fig. 4). Thermo-acoustic parametric analysis was used to develop and evaluate the needed corrections, the most important of which involved the reversal of both CM valves (JT and fill) to have the valve stem volume at low (~30 mbar) pressure.

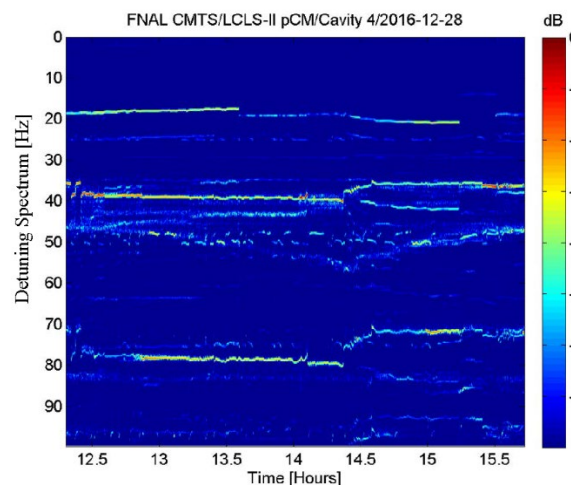


Figure 4: showing a four-hour duration cavity detuning spectrogram (difference between the cavity resonant frequency and nominal center frequency). The slow frequency drifts are correlated with the movement of cryogenics in the cryomodule and are consistent with TAO-generated frequencies.

This fix, together with improvements to the upstream gate valve cavity mounting and input piping improvements, was adequate to satisfy the +/- 10 Hz detuning microphonic-stability acceptance criteria that matches the  $Q_{ext}$ ,  $E_{acc}$ , and RF power-overhead.

Each CM is specified be operated in full ‘linac-mode’ during testing, i.e. all cavities frequency-locked at nominal integrated gradient for at least 10 hours. In practice, this has not been routinely achieved as 1) the cavity resonance stabilization is not mature enough to allow all cavities to be frequency-locked and 2) (for JLab) the cryogenic capacity of CMTF is inadequate to carry the full CM heat load.

Active compensation using the piezo-driven fast cavity tuner is foreseen, as the microphonic disturbance level in the SLAC tunnel may be different than in the test facilities. The tuner control / low level RF system provides the capability to deploy fast mechanical compensation if needed. Testing [35] demonstrated a factor 3 reduction in detuning.

Content from this work may be used under the terms of the CC BY 3.0 licence (© 2019). Any distribution of this work must maintain attribution to the author(s), title of the work, publisher, and DOI.

## Shipping

After CM acceptance testing is complete, each CM is shipped to the SLAC accelerator enclosure for installation. The cryomodules are integrated into long strings to await cool down and commissioning, which may be 2 – 3 years after testing.

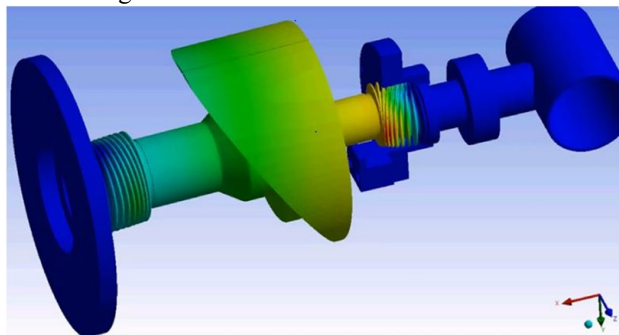


Figure 5: Mechanical model of the articulated FPC, showing the central DN100 6-inch conflat flange pair (middle of the figure). A section of beam pipe is shown in blue in the upper right side of the figure and the large insulating vacuum tank flange is shown on the left.

At the start of LCLS-II CM shipments to SLAC, two severe beamline loss-of-vacuum incidents occurred. These were traced to two shortcomings: 1) semi-trailer shipping frame springs were too stiff and 2) the FPC central ‘floating flange’ was insufficiently restrained and showed resonantly driven motion. [36, 37] In both incidents the vulnerable component which failed was the cold-side FPC flexible bellows (Fig. 5). The coaxial FPC is articulated and is designed to withstand ~10 mm of lateral offset from CM cool down. The central DN100 conflat flange pair and its surrounding thermal anchor shroud make up a roughly 5 kg central segment of the articulated assembly that does not have a mechanically stiff connection and oscillates at roughly 15 Hz natural frequency (warm and cold-side bellows under vacuum). Figure 5 shows the distortion of the FPC during road transport. The bellows shown on the right side cracked after a few thousand 6 mm peak – to – peak movements, a number easily exceeded in the initial transports. Subsequent bench testing of the bellows, heat treated and brazed in a manner similar to these, showed the same crack failures following similar integrated motion.

The disturbance to the FPC was exacerbated because the natural oscillation frequency of the truck-trailer transport frame was similar to its own natural frequency. This was readily fixed by adjusting the suspension spring scheme to reduce (2x) the transport frame frequency thus decoupling the resonantly-driven motion caused by the truck. In addition, a small neoprene spacer is clamped to the conflat flange assembly to limit the amplitude of motion. Installation of this can be awkward because it must be placed inside the completed CM after testing through the side-mounted tuner access ports and removed upon arrival at SLAC. This delicate process has been done many times but is prone to mishap because the inside of the CM is quite congested, and on one occasion the removal process failed and the CM beamline was damaged.

Initial shipments also showed flaws in cold mass fastener assembly with some fasteners becoming loose or undone. A complete fastener inventory and assembly protocol review was done with specific attention paid to thermal-anchor fasteners as these often rely on uniformly squeezed indium conduction gaskets. Following the review and implementation of corrections, no further fastener problems have been observed [30].

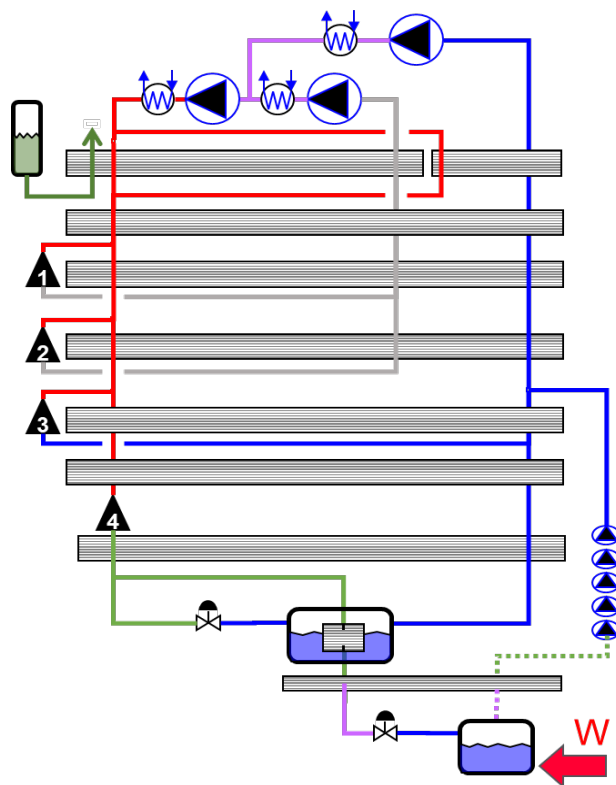


Figure 6: Single Cryoplant Process Flow Diagram, with room temperature at the top and 2K at the bottom. It shows the liquid nitrogen precooling (upper left), series/parallel high power warm compressors (top), expansion turbines (left), cold-box heat exchangers (8 each), sub-cooler vessel and heat exchanger, JT expansion valves (bottom, one in the cryoplant and one in CM), cold compressors (lower right). The cavity tanks are shown in the lower right with a red W to indicate heat from SRF.

## CRYOPLANT

Figure 6 shows the Process Flow Diagram of helium refrigerator equipped with five-stages of cold compression [7]. The design is optimum for a CW linac with high 2.0 K heat load and each refrigerator has mass-flow capability of 215 g/s. Table 6 shows the expected LCLS-II and LCLS-II-HE heat loads.

## PLANS

### Linac Integration

The L2 linac segment, 12 CM, (Fig. 1) is complete and interconnect welding is underway. We expect L3, 20 CM, to be complete until the end of 2019 and LCLS-II to be ready for initial commissioning and cryogenic testing in

summer 2020. Beam operation will start about one year later.

Table 6: Cryogenic System Heat static and dynamic loads for the three circuits, 70K shield, 5-8 K low-temperature intercept and 2.0 K inner circuit. The ultimate (LCLS-II-HE) total 2K load is anticipated to be 7.13kW, with a 12% margin below the dual cryoplant 8kW capacity.

Load	Circuit			Unit
	70	5-8	2	
<b>LCLS-II</b>				<b>K</b>
CM static heat	4.56	0.63	0.26	(kW)
CM dynamic heat	3.22	0.27	3.02	(kW)
CDS heat	4.29	0.21	0.25	(kW)
<i>Total</i>	<i>12.06</i>	<i>1.11</i>	<i>3.53</i>	<i>(kW)</i>
Total mass flow	115.6	58.0	174.6	(g/s)
<b>LCLS-II-HE</b>				
CM static heat	7.02	0.97	0.41	(kW)
CM dynamic heat	5.04	0.43	6.40	(kW)
CDS heat	8.37	0.36	0.32	(kW)
<i>Total</i>	<i>17.64</i>	<i>1.63</i>	<i>7.13</i>	<i>(kW)</i>

### LCLS-II-HE Plans

Studies aimed at high gradient are motivated by user-driven science up to 12.8keV Xray energy, more than double the Xray energy of LCLS-II (5keV). Roughly another 300 m of the SLAC accelerator enclosure was cleared of equipment and LCLS-II-HE planning is to install 20 CM in this area. These CM will contain cavities operating at an average  $E_{acc}$  of 20.8 MV/m (166 MV total per CM) and will roughly double the beam energy of LCLS-II to 8 GeV.

Single cell R&D [38] has been very encouraging and various doping schemes have shown above 30 MV/m and very good Q0. Work is now underway to extend this to nine cell cavities until the end of 2019 when an updated doping recipe will be provided to cavity vendors. To achieve 20.8 MV/m in the CM, the VT acceptance threshold is set to > 23 MV/m, 4 MV/m above the LCLS-II VT threshold.

### Plasma Cleaning

Loss of cavity beamline vacuum integrity was the most severe impact experienced and such an event requires full extraction and disassembly of the cold-mass and eventual cavity re-rinsing and reconstruction in the clean-room string assembly area. For future work, if the loss of vacuum is not too fast and vacuum integrity can be readily restored, we will consider treatment of the cavities using reactive chemical plasma processing as pioneered at SNS [39]. Initial testing of the technique to LCLS-II cavities is very promising [40].

## SUMMARY

LCLS-II is the first large CW linac based on the TESLA/ILC/XFEL technology. Cryomodule gradient and heat load performance is very encouraging for future CW applications, a credit to the innovative doping technique. The technique is expected to mature in the coming years leading to further application of SRF with both high gradient and low heat load performance.

## ACKNOWLEDGEMENTS

Completion of the LCLS-II linac was made possible through the efforts of the combined US Office of Science accelerator lab complex. The technical leadership at Fermilab and JLab, where all the components were brought together and tested, deserves special recognition: Ed Daly, Camille Ginsburg, Joe Preble, Rich Stanek, Dana Arenius, John Hogan, and Arkadiy Klebaner. At SLAC, the team led by Andrew Burrill deserves special recognition for their work to integrate it all. This project could not have been executed without close and effective collaboration with DESY (Hans Weise), CEA/Saclay (Olivier Napoly) and Cornell (Matthias Liepe).

## REFERENCES

- [1] J. Galayda, "LCLS-II: A High Power Upgrade to the LCLS", in *Proc. 9th Int. Particle Accelerator Conf. (IPAC'18)*, Vancouver, BC, Canada, Apr.-May 2018, pp. 18-23. doi:10.18429/JACoW-IPAC2018-MOYGB2
- [2] C. Bostedt *et al.*, "Linac Coherent Light Source: The first five years", *Reviews of Modern Physics*, 88, 2016. doi:10.1103/revmodphys.88.015007
- [3] C. Adolphsen *et al.*, "The International Linear Collider Technical Design Report - Volume 3.I: Accelerator R&D in the Technical Design Phase", ILC-REPORT-2013-040, Jun. 2013.
- [4] R. Brinkmann *et al.*, "TESLA Technical Design Report," DESY-2001-011, Mar. 2001.
- [5] T. Behnke *et al.*, "The International Linear Collider Technical Design Report - Volume 1: Executive Summary", ILC-REPORT-2013-040, Jun. 2013.
- [6] A. Grassellino, *et al.*, "Nitrogen and argon doping of niobium for superconducting radio frequency cavities: a pathway to highly efficient accelerating structures", *Superconductor Science and Technology*, vol. 26, No 10, p 102001, Aug. 2013. doi.org/10.1088/0953-2048/26/10/102001
- [7] V. Rao *et al.*, "Commissioning of helium refrigeration system at JLab for 12 GeV", *AIP Conference Proceedings* 1573, 944 (2014). doi.org/10.1063/1.4860806
- [8] A. Dallesandro, *et al.*, "Thermodynamic Analyses of the LCLS-II Cryogenic Distribution System", arXiv:1704.08339, 10.1109/TASC.2016.2646478
- [9] H. Weise and W. Decking, "Commissioning and First Lasing of the European XFEL", in *Proc. of 38th International Free Electron Laser Conference (FEL2017)*, Santa Fe, NM, USA, Aug 2017, p9-13. doi:10.18429/JACoW-FEL2017-MOC03
- [10] T. Raubenheimer, "The LCLS-II-HE, A High Energy Upgrade of the LCLS-II", in *Proc. 60th ICFE Advanced Beam Dynamics Workshop on Future Light Sources (FLS2018)*, Shanghai, China, p 6-11. doi:10.18429/JACoW-FLS2018-MOP1WA02
- [11] A. Crawford *et al.*, "The Joint High Q0 R&D Program for LCLS-II", in *Proc. of 5th International Particle Accelerator Conference IPAC2014*, Dresden, Germany, June 2014, p 2627-2630, doi.org/10.18429/JACoW-IPAC2014-WEPRI062

- [12] R. L. Geng, "Overview of ILC High Gradient Cavity R&D at Jefferson Lab," in *Proc. of 15<sup>th</sup> Intl Conf on RF Superconductivity (SRF2011)*, Chicago, IL USA, 2011, p. 74.
- [13] W. Singer, *et al.*, "Production of superconducting 1.3-GHz cavities for the European X-ray Free Electron Laser", *Phys. Rev. Accel. Beams* 19, 092001, doi:10.1103/PhysRevAccelBeams.19.092001
- [14] D. Gonnella *et al.*, "Industrialization of the nitrogen-doping preparation for SRF cavities for LCLS-II", *Nucl. Inst. Meth. A*, vol. 883, pp. 143-150, Mar. 2018, doi.org/10.1016/j.nima.2017.11.047
- [15] M. Liepe, *et al.*, "LCLS-II SRF Cavity Processing Protocol Development and Baseline Cavity Performance Demonstration", in *proc 17<sup>th</sup> Intl Conf on RF Superconductivity (SRF2015)*, Whistler, BC, Canada, Sept. 2015, pp. 159-163, doi:10.18429/JACoW-SRF2015-MOPB033
- [16] A. Palczewski, *et al.*, "Rework Recipe Development, Analysis and Results of Select 9-Cell Cavities for LCLS-II" in *proc 9th International Particle Accelerator Conference IPAC2018*, Vancouver, BC, Canada, Apr-May 2018, pp. 3968-3971, doi.org/10.18429/JACoW-IPAC2018-THPAL140
- [17] M. Martinello, *et al.*, "Effect of interstitial impurities on the field dependent microwave surface resistance of niobium", *Appl. Phys. Lett.* 109, 062601 (2016). doi:10.1063/1.4960801
- [18] A. Romanenko, A. Grassellino, O. Melnychuk, and D. A. Sergatskov, "Dependence of the residual surface resistance of superconducting radio frequency cavities on the cooling dynamics around Tc", *J. Appl. Phys.* 115, 184903 (2014). Doi:10.1063/1.4875655
- [19] S. Posen, *et al.*, "Efficient expulsion of magnetic flux in superconducting radiofrequency cavities for high Q0 applications", *J. App. Phys.* 119, 213903 (2016), doi:10.1063/1.4953087
- [20] Posen "Flux Expulsion Lessons Learned from LCLS-II", presented at 19<sup>th</sup> Intl. Conf. on RF Superconductivity (SRF'19), Dresden, Germany, July 2019, paper TUP039, this conference.
- [21] H. Quack, C. Haberstroh, and R. Langebach, "Fast cooldown of the two strings of the LCLS-II linac with increased mass flow rate", SLAC internal report, 2018.
- [22] S. Posen *et al.*, "The Role of Magnetic Flux Expulsion to Reach Q0>3e10 in SRF Cryomodules", *Phys. Rev. Accel. Beams* 22, 032001 (2019). doi.org/10.1103/PhysRevAccelBeams.22.032001
- [23] S. K. Chandrasekaran and A. C. Crawford, "Demagnetization of a complete superconducting radiofrequency cryomodule: Theory and practice", *IEEE Trans. Appl. Supercond.* 27, 1 (2017). doi:10.1109/TASC.2016.2635803
- [24] S. K. Chandrasekaran, A. Grassellino, C. Grimm, G. Wu, "Magnetic Field Management in LCLS-II 1.3 GHz Cryomodules" in *Proc. of 28<sup>th</sup> Linear Accelerator Conference (LINAC'16)*, East Lansing, MI, USA, Sept. 2016, pp. 527-530, doi:10.18429/JACoW-LINAC2016-TUPLR027
- [25] G. Cheng *et al.*, "Magnetic Hygiene Control on LCLS-II Fabricated at JLab," in *Proc. of 18<sup>th</sup> Intl Conf on RF Superconductivity (SRF2017)*, Lanzhou, China, July 2017, pp.153-157. doi:10.18429/JACoW-SRF2017-MOPB044
- [26] T. Peterson, *et al.*, "LCLS-II 1.3 GHz Cryomodule Design – Modified TESLA-Style Cryomodule for CW Operation", in *Proc. of 17<sup>th</sup> Intl Conf on RF Superconductivity (SRF2015)*, Whistler, BC, Canada, Sept. 2015, pp. 1417-1421, doi:10.18429/JACoW-SRF2015-THPB119
- [27] R. A. Legg, *et al.*, "LCLS-II Cryomodule Production at JLab", in *Proc. of 18<sup>th</sup> Intl Conf on RF Superconductivity (SRF2017)*, Lanzhou, China, July 2017, pp. 163-167. doi:10.18429/JACoW-SRF2017-MOPB046
- [28] C. Hovater *et al.*, "Operation of the CEBAF 100 MV Cryomodules", in *Proc. of 28<sup>th</sup> Linear Accelerator Conf. (LINAC'16)*, East Lansing, MI, USA, Sep. 2016, doi:10.18429/JACoW-LINAC2016-MOOP11
- [29] M. Santana Leitner, L. Ge, Z. Li, C. Xu, C. Adolphsen, M. Ross, M. Carrasco, *International Journal of Modern Physics: Conference Series*, Vol. 44, 2016, pp. 1660209, doi:10.1142/S201019451660209X
- [30] T. Arkan, *et al.*, "LCLS-II Cryomodules Production at Fermilab", in *Proc. of 9th International Particle Accelerator Conference IPAC2018*, Vancouver, BC, Canada, May 2018, doi:10.18429/JACoW-IPAC2018-WEPMK010
- [31] P. Ylä-Oijala, "Electron multipacting in TESLA cavities and input couplers", *Particle Accelerators*, Vol. 63, 105, 1999.
- [32] M. Checchin *et al.*, "Quench-Induced Degradation of the Quality Factor in Superconducting Resonators", *Phys. Rev. Applied* 5, 044019, 2016. doi:10.1103/PhysRevApplied.5.044019
- [33] S. Posen, "Cryomodule Measurements in Preparation for LCLS-II HE", presented at 19<sup>th</sup> Intl. Conf. on RF Superconductivity (SRF'19), Dresden, Germany, July 2019, paper TUP038, this conference.
- [34] B J Hansen *et al.*, "Effects of thermal acoustic oscillations on LCLS-II cryomodule testing", *IOP Conf. Ser.: Mater. Sci. Eng.* Vol. 278, pp. 012188, 2017, doi.org/10.1088/1757-899X/278/1/012188
- [35] J. Holzbauer, *et al.*, "Active Microphonics Compensation for LCLS-II", in *Proc. of 9th International Particle Accelerator Conference IPAC2018*, Vancouver, BC, Canada, May 2018 doi:10.18429/JACoW-IPAC2018-WEPMLO07
- [36] J.P. Holzbauer, "LCLS-II Cryomodule Transportation: Failures, Successes, and Lessons Learned", presented at 19<sup>th</sup> Intl. Conf. on RF Superconductivity (SRF'19), Dresden, Germany, July 2019, paper MOP090, this conference.
- [37] N. Huque, E. Daly, "LCLS-II Cryomodule Shipping: Issues and Solutions", presented at 19<sup>th</sup> Intl. Conf. on RF Superconductivity (SRF'19), Dresden, Germany, July 2019, paper TUP094, this conference.
- [38] D. Gonnella, "The LCLS-II HE High Q and Gradient R&D Program", presented at 19<sup>th</sup> Intl. Conf. on RF Superconductivity (SRF'19), Dresden, Germany, July 2019, paper MOP045, this conference.
- [39] M. Doleans, "Ignition and monitoring technique for plasma processing of multicell superconducting radio-frequency cavities", *Journal of Applied Physics* vol. 120, pp.243301, 2016 doi.org/10.1063/1.4972838
- [40] B. Giaccone, "Plasma Processing of LCLS-II Cavities", presented at 19<sup>th</sup> Intl. Conf. on RF Superconductivity (SRF'19), Dresden, Germany, July 2019, paper FRCAB7, this conference.